How to cite: *Angew. Chem. Int. Ed.* **2021**, *60*, 20383 – 20390
International Edition: doi.org/10.1002/anie.202106263
German Edition: doi.org/10.1002/ange.202106263

VIP **Gas Separation** *Very Important Paper*

Benchmark Acetylene Binding Affinity and Separation through Induced Fit in a Flexible Hybrid Ultramicroporous Material

Mohana Shivanna, Ken-ichi Otake, Bai-Qiao Song, Lisa M. van Wyk, Qing-Yuan Yang, Naveen Kumar, Wesley K. Feldmann, Tony Pham, Shanelle Suepaul, Brian Space, Leonard J. Barbour, Susumu Kitagawa, and Michael J. Zaworotko**

Abstract: *Structural changes at the active site of an enzyme induced by binding to a substrate molecule can result in enhanced activity in biological systems. Herein, we report that the new hybrid ultramicroporous material sql-SIFSIX-bpe-Zn exhibits an induced fit binding mechanism when exposed to acetylene, C_2H_2. The resulting phase change affords exceptionally strong C_2H_2 binding that in turn enables highly selective C_2H_2/C_2H_4 and C_2H_2/CO_2 separation demonstrated by dynamic breakthrough experiments. sql-SIFSIX-bpe-Zn was observed to exhibit at least four phases: as-synthesised (α); activated (β); and C_2H_2 induced phases (β' and γ). sql-SIFSIX-bpe-Zn-β exhibited strong affinity for C_2H_2 at ambient conditions as demonstrated by benchmark isosteric heat of adsorption (Q_{st}) of 67.5 kJ mol^{-1} validated through in situ pressure gradient differential scanning calorimetry (PG-DSC). Further, in situ characterisation and DFT calculations provide insight into the mechanism of the C_2H_2 induced fit transformation, binding positions and the nature of host-guest and guest-guest interactions.*

Introduction

The induced fit mechanism is a well-known process for the formation of enzyme-substrate complexes that enhance activity.[1] In this phenomenon, the enzyme active site undergoes a structural transformation to optimize the binding site for a specific substrate (Scheme 1a). Induced fit plays an important role in biological processes such as signal transduction, signal amplification and others.[2] Whereas induced fit is prominent in enzymatic reactions, it is rare and poorly understood in the context of crystalline porous materials, where such behaviour could result in enhanced selectivity to enable challenging gas capture or purification processes.[3] Metal organic materials (MOMs)[4] such as metal organic frameworks (MOFs),[5] porous coordination polymers (PCPs)[6] and hybrid ultramicroporous materials (HUMs)[7] are typically sustained by linker ligands and metal-based

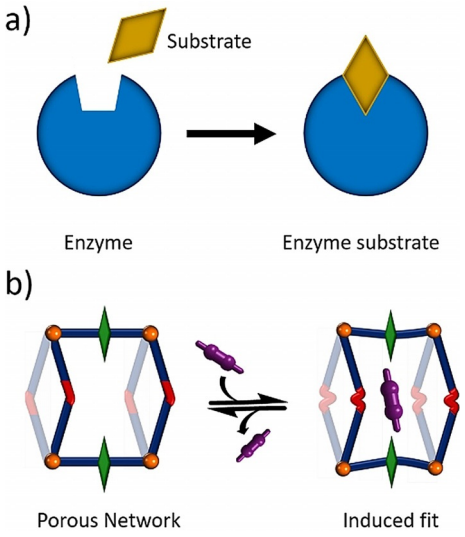

Scheme 1. Induced fit transformations. a) Enzyme active sites can undergo structural changes to better fit a substrate and enhance activity. b) A stimulus responsive ultramicroporous physisorbent that exhibits a structural transformation induced by a sorbate would be expected to offer enhanced binding energy and in turn enable better separations.

[*] Dr. M. Shivanna, Dr. B.-Q. Song, Dr. Q.-Y. Yang, N. Kumar, Prof. M. J. Zaworotko
Department of Chemical Sciences, Bernal Institute, University of Limerick
Limerick V94 T9PX (Republic of Ireland)
E-mail: Michael.Zaworotko@ul.ie
Dr. M. Shivanna, Dr. K. Otake, Prof. S. Kitagawa
Institute for Integrated Cell-Material Sciences, Kyoto University Institute for Advanced Study, Kyoto University
Yoshida Ushinomiya-cho, Sakyo-ku, Kyoto 606-8501 (Japan)
E-mail: kitagawa@icems.kyoto-u.ac.jp
L. M. van Wyk, Dr. W. K. Feldmann, Prof. L. J. Barbour
Department of Chemistry and Polymer Science, Stellenbosch University
Matieland 7602 (South Africa)
Dr. T. Pham, S. Suepaul, Prof. B. Space
Department of Chemistry, University of South Florida
4202 East Fowler Avenue, Tampa, FL 33620 (USA)
Dr. T. Pham
Department of Chemistry, Biochemistry, and Physics, The University of Tampa
401 West Kennedy Boulevard, Tampa, FL 33606-1490 (USA)
Supporting information and the ORCID identification number(s) for the author(s) of this article can be found under: https://doi.org/10.1002/anie.202106263.

nodes and can overcome the limitations of traditional classes of porous materials such as zeolites.[8] Such porous coordination networks offer a high degree modularity which makes them amenable to design from first principles using crystal engineering strategies.[9] A small subset of MOFs and HUMs can undergo structural transformation upon exposure to stimuli[10] such as heat, gas/vapor or light could therefore be relevant for application in storage,[11] separations,[12] catalysis,[13] molecular sensor[14] and drug release.[15] There are at least 150 MOFs[16] that have been shown to exhibit flexibility among the >75000 reported MOFs.[17] The origin of flexibility has been well studied and is attributed to various mechanism such as breathing, swelling, switching, shape memory and others.[10a,b,18] To our knowledge, there are only five previous reports of induced fit driven by gas sorption.[19]

For example, Rosseinsky et al.[19b] reported a flexible framework, (ZnGGH-1·DMF-H_2O) (GGH = tripeptide glycine-glycine-l-histidine) which changes conformation to adapt to the shape and size of specific guest thanks to the flexible skeleton of the organic linker. A CPL network, $[Cu_2(pzdc)_2(bpy)]$ (pzdc = pyrazine-2,3-dicarboxylate and bpy = 4,4-bipyridine), was found to contract upon heating the as synthesised phase; further contraction occurred with benzene occupying channels. This induced fit is attributed to isomerisation from square pyramidal to square planar geometry.[19d] Similarly, a flexible chemisorbent, $[Zn_3(OH)_2(btca)_2]$ (H_2btca = benzotriazole-5-carboxylic acid), contracted after activation from its as synthesised phase and further contraction occurred following C_2H_2 adsorption with binding affinity of 47.6 kJ mol^{-1}.[19c] The mechanism of contraction was driven by the binding affinity of C_2H_2 towards unsaturated Zn centres and self-adaptive shrinkage of the framework. Whereas physisorbents can exhibit C_2H_2 induced structural transformations,[20] flexible physisorbents that offer induced fit mechanisms for C_2H_2 (Scheme 1b) have not yet been reported. We consider this to be a desirable objective since high binding energy, low regeneration energy and good separation performance would be anticipated from such sorbents.

Among commodity gases, high purity C_2H_2 is the starting material for industrially relevant products such as plastics, vinyl compounds, acrylic derivatives and α-ethyl alcohols.[20f] Currently, C_2H_2 is produced by the partial combustion of methane or through the cracking of hydrocarbons. However, this process generates impurities such as C_2H_4 and CO_2. The similar quadruple moments and kinetic diameters (Table S1) of these gases makes the process of selective capture of one gas (for example, C_2H_2) from the other gases difficult and energy intensive. In this context, rigid MOFs with high C_2H_2 affinity have been reported with binding driven by open metal sites,[21] hydrogen bonding,[22] synergistic effect of open metal sites and electronegative sites[23] or acidic/basic functional groups.[24] HUMs[7a] have also demonstrated high C_2H_2 binding affinity over other gases such as C_2H_4,[25] CO_2[26] and other hydrocarbon mixtures.[27] For example, Li et al. achieved benchmark C_2H_2 selectivity over C_2H_4 using SIFSIX-14-Cu-i.[25] The high performance exhibited by HUMs has been attributed to ultramicropores (<0.7 nm), strong electrostatic interactions with the inorganic "pillars" (SiF_6^{2-} or SIFSIX) and pore structure. Overall, the current C_2H_2 benchmark for isosteric heat of adsorption (Q_{st}), ≈60 kJ mol^{-1} at low loading, rests with the rigid ultramicroporous MOF known as NKMOF-1-Ni.[28] The binding affinity of a sorbent can provide a guide to its separation performance for a specific gas in a mixture of gases. Flexible physisorbents which exhibits induced fit have the advantage over chemisorbents. This is because flexible framework can recognise only specific guest molecule vs. different multiple guest and then adopt new configuration from their original structure especially those designed with special binding sites (for example, originating from inorganic pillar) and flexible skeleton from ligand. That newly transformed structure induces tight cavity for that specific guest, combining strong interactions lead to extraordinary guest binding affinity with low regeneration energy. Herein we report that the use of an inorganic pillar, SiF_6^{2-} and a flexible dipyridyl linker ligand affords a new flexible physisorbent $[Zn(SiF_6)(1,2\text{-bis}(4\text{-pyridyl})\text{ethane})_2]_n$, which exhibits induced fit in single crystal to single (SC-SC) fashion when exposed to C_2H_2 under ambient conditions. In-situ X-ray diffraction was used to study the reversibility of the phase transformations and the switching mechanisms driven by C_2H_2 and CO_2 loading at 195 K. As revealed herein, the observed SC-SC transformations are driven by host-guest interactions with the inorganic pillar and therefore differ from the previously reported examples of induced fit binding (Table S2).

Results and Discussion

$[Zn(SiF_6)(bpe)_2]_n$ exists as a 3D pcu or 2D sql network when prepared from 1,2-bis(4-pyridyl) ethane and $ZnSiF_6^{2-}$ using different solvent combinations. Chloroform and methanol resulted in the pcu variant (Figure S1). Single-crystal X-ray diffraction (SC-XRD) revealed that the organic linker adopts the trans- conformation and orthorhombic space group Ibam (Table S3). Single crystals were unstable to loss of guest, making it a 1st generation PCP.[6] When pure methanol was used, single crystals of the sql variant were harvested. Crystals were observed to be stable when removed from other liquor and SC-XRD revealed that bpe linkers are in cis- conformation and the monoclinic space group *C*2/*c* was adopted (Table S3). The ability of bpe to exhibit conformational flexibility is long known.[29] The sql phase (sql-SIFSIX-bpe-Zn-α; Figure 1) exhibits 18% guest-accessible volume which is occupied by methanol molecules. The void space was calculated with a probe radius of 1.2 Å and a grid spacing of 0.7 Å. Single crystals of the activated or β phase (sql-SIFSIX-bpe-Zn-β) were obtained by heating the α phase at 353 K under vacuum for 12 h.

The β phase transformed to the triclinic space group P-1 with a density of 1.351 g cm^{-3} well below that of the α phase (1.523 g cm^{-3}). The crystal structures of the β phase revealed that its 2D networks are distorted and the guest-accessible volume is reduced to 14% (Figures 2a and b). The phase transformation from α to β was also studied by in situ variable temperature powder X-ray diffraction (PXRD) at intervals of 10 °C every 10 min, which revealed that transformation

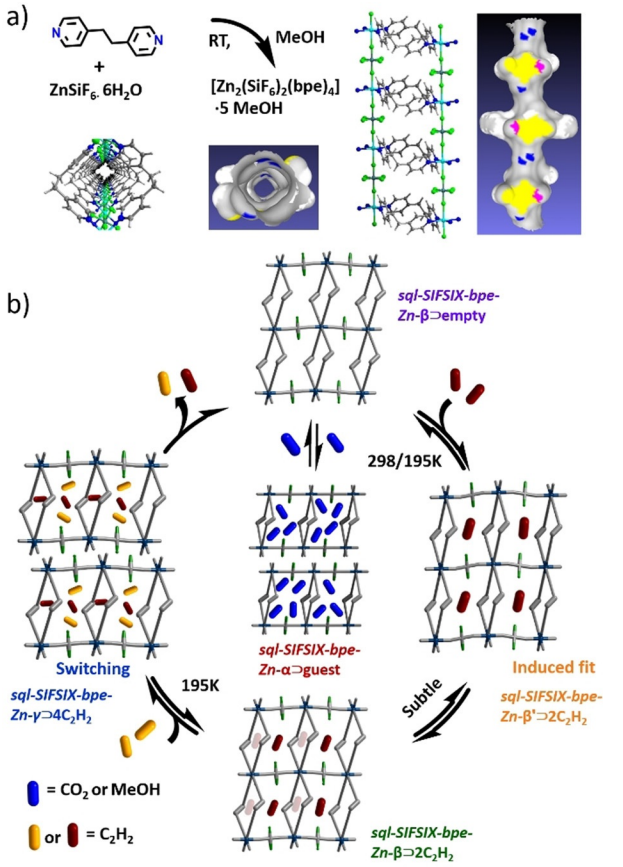

Figure 1. Schematic representation of the synthesis and structural transformations of sql-SIFSIX-bpe-Zn. a) Structure of the organic linker (1,2-bis(4-pyridyl) ethane) and inorganic components (Zn^{2+} and SIFSIX pillar) that formed a 2D net with **sql** topology that exhibits channels. b) The as-synthesised phase, α, underwent reversible transformation to the β phase upon removal/insertion of MeOH or CO_2. C_2H_2 sorption induced another phase, $\beta' \supset 2C_2H_2$, which accommodated $2C_2H_2$ molecules. $\beta \supset 2C_2H_2$ can adsorb two additional C_2H_2 molecules within the layers at 195 K by a switching transformation from $\beta \supset 2C_2H_2$ to $\gamma \supset 4C_2H_2$. Upon desorption, reversible transformation from $\gamma \supset 4C_2H_2$ and $\beta \supset 2C_2H_2$ to β occurred at 195 K and 298 K, respectively.

occurred at 333 K (Figure S2). This phase change was also observed in differential scanning calorimetry (DSC) measurements as a small exothermic peak occurred at 333 K (Figure S3). Thermogravimetric analysis (TGA) indicated that both the α and β phases were stable up to 463 K with ≈13% weight loss for α, which corresponds to 5 MeOH molecules per unit cell that include one additional methanol from the surface of crystals (Figure S4).

To study the porosity of sql-SIFSIX-bpe-Zn, gas sorption isotherms were measured for CO_2 at 195 K, C_2H_2 at 195 K, and N_2 at 77 K. Prior to gas sorption measurements, the α phase was activated at 353 K under vacuum for 12 h. A stepped isotherm was observed for C_2H_2 adsorption at 195 K (Figure S8). A plateau from 0 to 40 $cm^3 g^{-1}$ (2 guests per unit cell) was observed upon increasing the pressure up to $p/p_0 = 0.01$, followed by a sudden increase in uptake to 82 $cm^3 g^{-1}$ (4 guests per unit cell), which is the saturated uptake at $p/p_0 = 1$. In the case of CO_2 adsorption (Figure S9), a slight inflection was observed up to $p/p_0 = 0.008$ in the uptake range from 30 to 65 $cm^3 g^{-1}$. Saturated CO_2 uptake (80 $cm^3 g^{-1}$, 4 CO_2 per unit cell) was the same as that for C_2H_2 at $p/p_0 = 1$. In both isotherms, desorption matches the adsorption profile and the PXRD pattern after desorption indicates that the β phase is recovered (Figure S11). N_2 sorption revealed a typical type-I isotherm with saturated uptake limited to only 38 $cm^3 g^{-1}$ at $p/p_0 = 1$, which is approximately equal to 2 guests per unit cell (Figure S10).

To gain insight into the mechanism behind the stepped isotherm, in situ coincidence PXRD measurements during C_2H_2 and CO_2 adsorption at 195 K were conducted. A few selected adsorption and desorption points in each sorption profile in which significant phase change occurred are plotted in Figure 3. Diffraction patterns from point 6 to 87 are shown for C_2H_2 at 195 K in Figure 3a. C_2H_2 sorption revealed that the β phase remains to point 44 with an uptake of 40 $cm^3 g^{-1}$. Further increase in pressure afforded new peaks after the step that we attribute to the structural transformation from β to a new more open phase, γ (sql-SISIX-bpe-Zn-γ). The fully loaded γ phase remains unchanged during further adsorption (from point 46 to 55) and desorption (from point 78 to 87). Following the desorption process, we observed that γ returned to β as revealed by Figure 3a. With respect to in situ CO_2 sorption, the diffraction patterns indicated that transformation occurs from β to α in a reversible manner. Selected patterns from point 1 to 77 are plotted in Figure 3b. At point 12, new PXRD pattern emerged, which remained unchanged to $p/p_0 = 1$ and after desorption. The PXRD pattern at fully loaded point 33 matches the α phase. Finally, after desorption, α returns to β as shown in Figure 3b. In-situ PXRD patterns were also measured during N_2 sorption at 77 K (Figure 3c). The PXRD patterns indicate that N_2 does not induce a phase change during sorption, presumably because of its weaker interactions with the sorbent. This can also be inferred from the uptake reaching 38 $cm^3 g^{-1}$ at $p/p_0 = 1$, which is half of the uptake vs. C_2H_2 and CO_2. To identify guest binding sites upon C_2H_2 sorption in situ gas loading experiments were conducted on single crystals. A suitable single crystal was selected for these studies and activated in situ at 80 °C for 2 hrs under vacuum. C_2H_2 was dosed into the capillary when the temperature had reached 298 K. Cooling to 195 K revealed that transformation from β to γ occurred within 30 mins, as confirmed by a change in unit cell parameters. SCXRD analysis revealed that the γ phase retained the same space group as the β phase and that there are four distinct C_2H_2 binding sites (Table S3 and Figure S15). The occupancy of each C_2H_2 site was refined at 0.5, which we attribute to slow loading kinetics. The calculated PXRD pattern for the γ phase matches the in situ PXRD pattern at adsorption point 55 as revealed by Figure 3a and Figure S14. The transformation from the β to γ phase resulted in reduced quality data vs. that obtained for the β phase at 298 K ($R = 16\%$, $wR2 = 45\%$).

The nature of the pore size and chemistry of the β phase prompted us to explore gas sorption of C_2H_2, C_2H_4, CH_4, C_2H_6, and CO_2 at 298 K. C_2H_2 exhibited strong affinity with sharp uptake at low pressures compared to the other four gases (Figure 4a and S16). The C_2H_2 uptake was 26 $cm^3 g^{-1}$ at $p/p_0 = 0.01$, reached close to saturation at a relatively low pressure ($p/p_0 = 0.1$) with an uptake of 38 $cm^3 g^{-1}$ and was

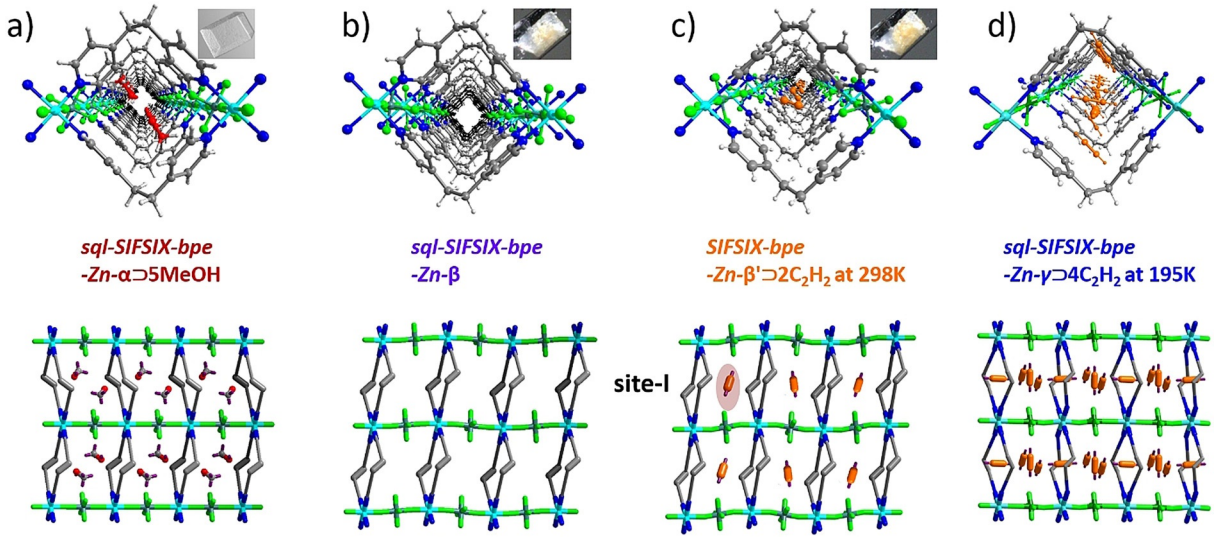

Figure 2. The phases of sql-SIFSIX-bpe-Zn studied by in situ single-crystal X-ray diffraction. a) The as-synthesized α phase exhibits 1D channels occupied by 5 methanol molecules per unit cell as determined by SCXRD and TGA. b) The α phase underwent transformation to the β phase upon heating at 353 K. This transformation was investigated by in situ variable temperature PXRD and in situ SC-XRD. c) and d) In-situ SCXRD measurements at 298 and 195 K enabled determination of the C_2H_2 binding sites in the β′ and γ crystal structures, respectively, which revealed a single binding site (site-I) in β′⊃$2C_2H_2$ and multiple binding sites in γ⊃$4C_2H_2$. The respective crystal photomicrographs of SC-SC transformations are presented in (a), (b) and (c).

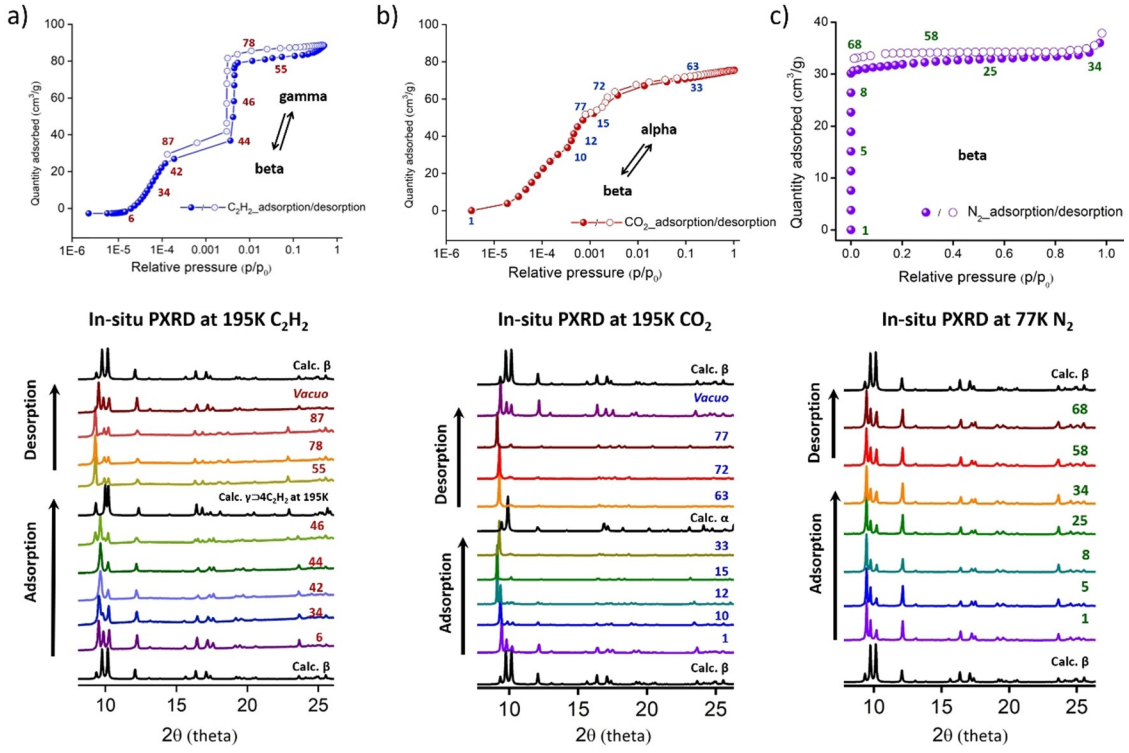

Figure 3. In-situ coincidence PXRD. Numbers in adsorption/desorption traces correspond to numbering of the PXRD patterns: a) In-situ PXRD measured at 195 K during C_2H_2 adsorption/desorption revealed a reversible switching transformation from β to γ. b) In-situ PXRD experiments conducted during CO_2 adsorption/desorption at 195 K revealed that switching occurred from β to α in reversible manner. c) In-situ PXRD measurements conducted under N_2 at 77 K revealed that the β phase remains unchanged during the adsorption/desorption.

saturated (40 $cm^3 g^{-1}$) at $p/p_0 = 1$. In contrast, the C_2H_4, C_2H_6 and CO_2 sorption isotherms exhibited negligible uptake at $p/p_0 = 0.01$ whereas increasing pressure to $p/p_0 = 0.1$ resulted in uptakes of 11, 5 and 24 $cm^3 g^{-1}$, respectively. The uptake capacity at $p/p_0 = 1$ was found to be 28, 18 and 40 $cm^3 g^{-1}$ for C_2H_4, C_2H_6 and CO_2, respectively. Interestingly, molecular sieving behaviour towards CH_4 was observed, with a saturated uptake of only 3 $cm^3 g^{-1}$ at $p/p_0 = 1$. When fully saturated at $p/$

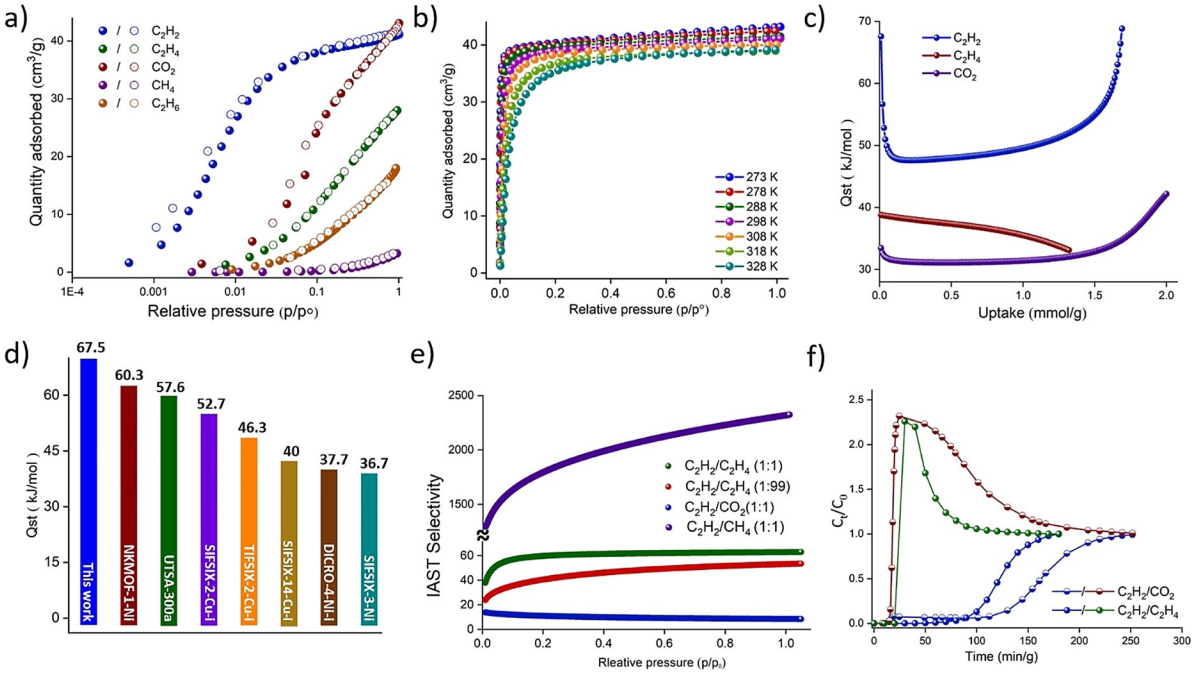

Figure 4. Pure component C_2H_2, C_2H_4, C_2H_6, CH_4, CO_2 sorption isotherms, their interaction energies and separation performance. a) C_2H_2, C_2H_4, CH_4, and CO_2 sorption isotherms for sql-SIFSIX-bpe-Zn measured at 298 K, plotted in log scale. b) C_2H_2 sorption isotherms measured at different temperatures in 10 °C intervals from 273 to 328 K. c) Isosteric heat of adsorption (Q_{st}) calculated from Clausius-Clapeyron equation for C_2H_2 (blue), CO_2 (purple), and C_2H_4 (red). d) C_2H_2 Q_{st} of sql-SIFSIX-bpe-Zn in this work and other benchmark materials. e) IAST selectivity calculated for C_2H_2/C_2H_4, C_2H_2/CH_4, and C_2H_2/CO_2 gas mixtures for various ratios at 298 K and pressures up to 1 bar. f) Breakthrough separation of C_2H_2/CO_2 and C_2H_2/C_2H_4 measured at 1:1 ratio under helium flow at 298 K.

$p_0 = 1$, the guest occupancy for C_2H_2, C_2H_4, C_2H_6 and CO_2 was observed to be on the order of 2, 1, 1 and 2 molecules per unit cell, respectively. Cycling experiments indicated that C_2H_2 sorption profiles were reproducible with the same uptake over 10 cycles (Figure S17). Sample regeneration was achieved by vacuum treatment at 313 K for 30 mins without additional heat. In order to calculate Q_{st}, we measured sorption at various temperatures ranging from 273 to 328 K in 5 °C or 10 °C intervals (Figures 4b, S18, S19). The resulting Q_{st} calculations on C_2H_2 sorption revealed that β offers a new benchmark for sorbent-C_2H_2 interaction energy (Figure 4c). A Q_{st} value of 67.5 kJ mol^{-1} was observed at zero loading, this value decreasing to ≈48 kJ mol^{-1} and then increased with uptake capacity. Conversely, C_2H_4, CH_4, and CO_2 exhibits low affinity with Q_{st} values of 38.4, 11, and 33.6 kJ mol^{-1}, respectively (Figures 4c and S23). The observed interaction energy for C_2H_2 exceeds previously reported materials as detailed in Figure 4d and Table S4, for example, SIFIX-3-Ni (Q_{st}, 36.7 kJ mol^{-1}),[26] SIFSIX-2-Cu-i (Q_{st}, 52.7 kJ mol^{-1}),[30] TIFSIX-2-Cu-i (Q_{st}, 46.3 kJ mol^{-1})[26,30] and UTSA-300a (Q_{st}, 57.6 kJ mol^{-1}),[20e] $Ni_3(pzdc)_2$ $(7Hade)_2$ (Q_{st}, 44.5 kJ mol^{-1}),[23] $Fe(pyz)Ni(CN)_4$ (Q_{st}, 32.8 kJ mol^{-1}),[31] $Co(pyz)Ni(CN)_4$ (Q_{st}, 45–65 kJ mol^{-1}),[32] ZUL-100 Q_{st}, 65.3 kJ mol^{-1}) and ZUL-200 (Q_{st}, 57.6 kJ mol^{-1}).[20b] Other approaches that focus upon chemisorption can exhibit higher energies such as the nano-trap MOF ATC-Cu, for which a Q_{st} of 79.1 kJ mol^{-1} driven by coordination between two metal centres was reported.[33] To further verify the energy of C_2H_2 sorption, we conducted in situ pressure gradient differential scanning calorimetry (PG-DSC) measurements. The enthalpy obtained for C_2H_2 was in good agreement with the Q_{st} obtained from the Clausius-Clapeyron equation (Figures 4c and S24).[34] To address gas mixture selectivity we conducted ideal adsorbed solution theory (IAST)[35] calculations. IAST calculations are not always well-suited for induced structural transformations but the subtle transformations upon C_2H_2 loading did not result in stepped or "S-shaped" isotherms, instead they appeared as Type-I isotherms. Unfortunately, selectivity calculations using breakthrough data were infeasible because of co-adsorption and steps. Calculated IAST selectivity values at 1 bar for both trace and bulk concentrations were as follows: C_2H_2/C_2H_4 (1:1, 62.8 and 1:99, 53.1), C_2H_2/CH_4 (2:1, 2426 and 1:1, 2302) and C_2H_2/CO_2 (1:1, 8.4) (Figure 4e and Table S4). The IAST selectivity for C_2H_2/C_2H_4 and C_2H_2/CO_2 can be compared to other leading sorbents (Table S4). TIFSIX-2-Cu-i has slightly higher selectivity for 1:99 C_2H_2/C_2H_4 (55) but is lower for 1:1 C_2H_2/C_2H_4 (45) and 1:1 C_2H_2/CO_2, (6.2) at 1:1.[26,30] Co-(pyz)$Ni(CN)_4$ offers higher selectivity for 1:1 C_2H_2/CO_2 (36.5) but is lower for 1:99 C_2H_2/C_2H_4 (24.2).[32] SIFSIX-3-Ni exhibited relatively low selectivity of 16.5, 17.6, 0.14 for C_2H_2/C_2H_4 (1:99 and 1:1) and C_2H_2/CO_2 (1:1), respectively.[26] A number of highly selective materials that were studied for one gas mixture only have recently been reported, for example, ATC-Cu (1:1 $C_2H_2/CO_2 = 53.6$),[33] $Ni_3(pzdc)_2$ $(7Hade)_2$ (1:99 $C_2H_2/C_2H_4 = 168$)[23] and $Fe(pyz)Ni(CN)_4$ (1:1 $C_2H_2/CO_2 = 24$).[31] In order to further investigate gas mixture separations, we conducted dynamic breakthrough experiments on 1:1 mixture upon Helium dilution. These

experiments revealed that the breakthrough time for C_2H_2/C_2H_4 was ≈1 h 15 mins whereas that for C_2H_2/CO_2 was ≈1 h 40 mins (Figure 4 f). C_2H_2 uptake (≈20 $cm^3 g^{-1}$) reached half of the total capacity (40 $cm^3 g^{-1}$) from sorption experiments and outlet purity was found to be ≈99 %. To determine the gate opening temperature for C_2H_2, C_2H_4 and CO_2, we conducted isobar experiments with increasing temperature from 195 K to 328 K (Figure S26). In the C_2H_2 isobar, the uptake capacity from 328 to 278 K remained almost constant with a value of 40 $cm^3 g^{-1}$ at $p/p_0 = 1$. A sudden step occurred from 268 to 258 K, when uptake capacity nearly doubled (≈77 $cm^3 g^{-1}$). Decreasing in temperature from 258 to 238 K resulted in C_2H_2 uptake gradually increasing to ≈82 $cm^3 g^{-1}$, a value that was maintained until 195 K. A similar sorption profile was observed for C_2H_4, but with a very low gate opening temperature. No step was observed from 328 to 238 K while a large step from 228 to 218 K with an uptake of 80 $cm^3 g^{-1}$ was seen. This type of switching isobar trend is rare in MOFs.[36] The CO_2 isobar exhibits a normal trend, showing a gradual increase in uptake from 40 to 82 $cm^3 g^{-1}$ with decrease in temperature from 328 to 195 K.

To gain insight into the sorption performance and benchmark interaction energy towards C_2H_2, we conducted in situ gas loading on single crystals, in situ coincidence PXRD and in situ FTIR measurements at 298 K (Figure 5). From in situ gas loading experiments, we obtained the structures of β′⊃2C_2H_2 and β⊃2C_2H_2 at less than $p/p_0 = 1$. In β′, C_2H_2 molecules were found to align between the SIFSIX pillars (Figure 5 c). In the β phase, C_2H_2 molecules were found to align between the SIFSIX pillars (site-I) and in adjacent cavities (site-II) (Figure 5 d). In-situ coincidence PXRD measurements from selected adsorption (1–22) and desorption points (49–65) are plotted in Figure 5 a. Point 1 indicates that the β phase remains unchanged. When the pressure is increased up to point 6, a slight difference in the peak intensity is observed at lower 2θ values, which nearly matches the calculated β′ powder pattern. Further increase in pressure up to point 18 produces a new PXRD pattern corresponding to the β⊃2C_2H_2 phase. After the desorption process, the pure β phase can be recovered as indicated in the calculated β powder pattern (Figure S11). In-situ FTIR study of C_2H_2 adsorption reveals two stretching bands that indicate two different types of C_2H_2 binding positions in the framework (Figure 5 b). At low pressures ($p/p_0 = 0.001$ at point 4), a band at 3200 cm^{-1} emerges, which corresponds to C_2H_2 at site-I. When the pressure is increased to point 20, another stretching band at 3311 cm^{-1} appears, which we attribute to C_2H_2 adsorbed at site-II. The two stretching bands are consistent with the binding positions identified in the in situ structures.

To obtain a better understanding of the interaction energy, we analysed the in situ structures obtained at 298 K. In β′⊃2C_2H_2, C_2H_2 molecules at site-I position form multiple C–H···F hydrogen bonding interactions ($D_{C\cdots F}$ = 2.199 Å, 2.200 Å, 2.240 Å, 2.675 Å) with the SIFSIX pillars (Figure 5 c). In β⊃2C_2H_2, C_2H_2 guests are also positioned at site-I with C–H···F hydrogen bonding interactions ($D_{C\cdots F}$ = 2.716 Å, 2.766 Å, 3.014 Å) (Figure 5 d). The C_2H_2 molecules at site-II in β⊃2C_2H_2 exhibit multiple interactions with the aromatic ligand (C–C···π with $D_{C\cdots C}$ = 2.517 Å, 2.615 Å and C–H···π with $D_{C\cdots C}$ = 3.448 Å, 3.353 Å) (Figure 5 e). There are also

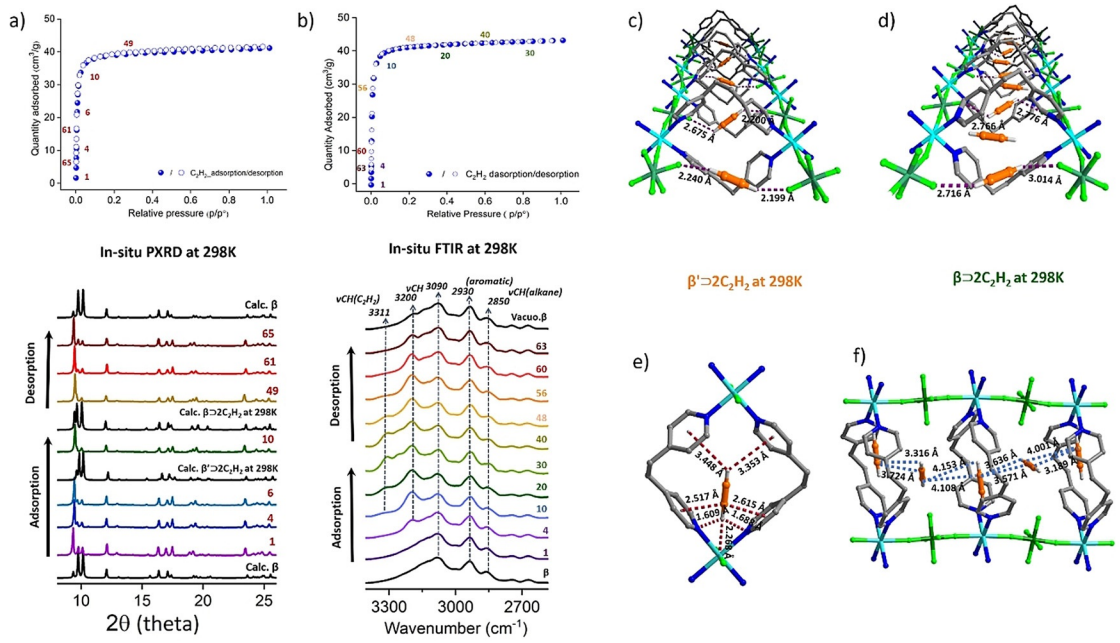

Figure 5. In-situ coincidence PXRD, FTIR and gas loading experiments at 298 K. Numbers in adsorption/desorption traces correspond to numbering of the PXRD patterns/FTIR spectra. a) In-situ PXRD during C_2H_2 adsorption/desorption at 298 K provides insight into phase transformations and the gas diffusion mechanisms at various pressures. b) In-situ FTIR measurements were conducted during C_2H_2 sorption at 298 K to gain insight into C_2H_2 stretching bands at different gas loading pressures. c) In-situ gas loading structure of β′⊃2C_2H_2 measured at 298 K. C_2H_2 molecules (orange/grey) were found to occupy the region between the SIFSIX pillars. d) In-situ structure of β⊃2C_2H_2 at 298 K and 1 bar with C_2H_2 occupying site-I and site-II. e) Illustration of the environment of C_2H_2 molecules in β⊃2C_2H_2, and f) Illustration of σ···π and π···π interactions in β⊃2C_2H_2.

intermolecular hydrogen bonding interactions between C_2H_2 molecules (σ···π, C–H···C with $D_{C\cdots C}=3.316$ Å, 4.153 Å, 3.636 Å and π···π, C–C···C with $D_{C\cdots C}=3.189$ Å, 3.571 Å, 3.724 Å, 4.108 Å) (Figure 5 f). DFT calculations support the experimentally determined structure of β′⊃2C_2H_2 with C_2H_2 molecules forming favourable interactions between two SIFSIX pillars ($D_{C\cdots F}=1.998$, 2.113, 2.151, and 2.644 Å) (Figure S31). C_2H_4 and CO_2 molecules align with the SIFSIX pillar in a less favourable perpendicular manner. The interaction distances between the SIFSIX pillar and both C_2H_4 molecules ($D_{C\cdots F}=2.31$, 2.53, 2.71, and 3.42 Å) and CO_2 molecules (C-O···F with $D_{O\cdots F}=2.57$ Å) are longer than those for C_2H_2 (Figure S32). For the β⊃2C_2H_2, the calculated binding positions of C_2H_2 also support the experimental results (Figure S33). The calculated binding energies of C_2H_2 in β′⊃2C_2H_2 and β⊃2C_2H_2 and the energy of transition from β⊃empty to β′⊃2C_2H_2 and β′⊃2C_2H_2 to β⊃2C_2H_2 were determined to be −48.26 and −32.87, −17.8, and +5.29 kJ mol^{-1}, respectively. These calculations suggest that β′ is more energetically favourable than β by about 5 kJ mol^{-1} and that the transition from β′ to β is driven by the heat released from adsorption of the C_2H_2 molecules. Further, to understand the mechanism of induced fit for C_2H_2, we analysed and compared crystal structures of β⊃empty, β′⊃2C_2H_2 and β⊃2C_2H_2. In β′⊃2C_2H_2, the alkane chain of the ligand undergoes distortion ($\measuredangle_{C\text{-}C\text{-}C}=113°$ to 123°), the rotation angle of SIFSIX pillar largely affected ($\measuredangle_{M\text{-}Si\text{-}F}=$ 82.63° to 97.36°) and metal to F of SIFSIX bond distances becomes longer ($D_{Zn\cdots F}=1.98$ to 2.19 Å and $D_{Si\cdots F}=1.55$ to 1.93 Å) (Figures S27 and S29). In β⊃empty, the alkane chain ($\measuredangle_{C\text{-}C\text{-}C}=116°$ to 118°), rotation angle of SIFISX pillar ($\measuredangle_{M\text{-}Si\text{-}F}=88.31°$ to 91.68°) and metal to F atom of SIFSIX bond distances ($D_{Zn\cdots F}=2.07$ to 2.09 Å and $D_{Si\cdots F}=1.72$ to 1.74 Å) were observed to be slightly distorted (Figures S27 and S28), similar to β⊃2C_2H_2. For example, angle of alkane chain ($\measuredangle_{C\text{-}C\text{-}C}=112°$ to 116°), angle of metal to SIFSIX ($\measuredangle_{M\text{-}Si\text{-}F}=87.01°$ to 92.98°) and bond distances of metal to F atom ($D_{Zn\cdots F}=2.09$ Å and $D_{Si\cdots F}=1.72$ Å) (Figures S27 and S30). The pore cavity of F to F interactions increased in β′⊃2C_2H_2 ($D_{F\cdots F}=7.02$ to 7.24 Å) than β⊃empty ($D_{F\cdots F}=6.87$ to 6.75 Å) and β⊃2C_2H_2 ($D_{F\cdots F}=6.84$ to 6.96 Å) (Figures S28 to S30). This analysis reveals that pore cavity in β′ structure is more suitable to accommodate C_2H_2 and energetically favourable than β. Therefore, we conclude that the following primary factors contribute to the induced fit mechanism in sql-SIFSIX-bpe-Zn: i) degree of freedom in the structure and electronic structure of the system; ii) multiple hydrogen bonding interactions between C_2H_2 molecules and SIFSIX pillars providing tighter binding site; iii) rotational motion of SIFSIX pillar and organic ligand that can undergo contortion.

Conclusion

In summary, herein we report a new 2D flexible ultramicroporous physisorbent, sql-SIFSIX-bpe-Zn, that exhibits induced fit specifically for C_2H_2 under ambient conditions and undergoes switching from open to more open phases induced by C_2H_2 and CO_2 adsorption at cryogenic temperatures. The induced fit transformation results in benchmark C_2H_2 binding affinity thanks to a tight binding site that enables multiple sorbent-sorbate interactions. High C_2H_2 selectivity and strong separation performance was found for C_2H_4 and CO_2 binary gas mixtures. In-situ characterization using PXRD, SC-XRD, synchrotron diffraction, FTIR, and PG-DSC measurements were used to elucidate the mechanism of induced fit and identify sorbate binding sites. The detailed in situ characterization results are supported by modelling studies provides insight that could be used to enable a new and general approach to the design of the next-generation porous physisorbents: flexible ultramicroporous sorbents that exhibit induced fit for of a specific gas molecule, resulting in a selectivity hitherto unseen in rigid porous physisorbents.

Acknowledgements

M.Z. thanks Science Foundation Ireland for funding of this research (SFI Awards 13/RP/B2549, 16/IA/4624). K.O. and S. Kitagawa acknowledge the financial support of KAKENHI, Grant-in-Aid for Scientific Research (S) (JP18H05262), and Early-Career Scientists (JP19K15584) from the Japan Society of the Promotion of Science (JSPS). Synchrotron XRD measurements were supported by the Japan Synchrotron Radiation Research Institute (JASRI) (Proposal Nos. 2018B1820, 2019A1600, 2019B1554). L.B. thanks the National Research Foundation of South Africa for financial support. We thank D. M. Franz and G. Beemer for preliminary DFT calculations, A. Bajpai for providing details of initial synthesis, and thank to Andrey. A. Bezrukov for drawing Figure 1. B.S. acknowledges the National Science Foundation (Award No. CHE-1152362), including support from the Major Research Instrumentation Program (Award No. CHE-1531590), the computational resources that were made available by a XSEDE Grant (No. TG-DMR090028), and the use of the services provided by Research Computing at the University of South Florida. Open access funding provided by IReL.

Conflict of Interest

The authors declare no conflict of interest.

Keywords: coordination polymers · C_2H_2/C_2H_4 and C_2H_2/CO_2 separation · induced fit mechanism · physisorption · ultramicroporous materials

[1] a) R. Domínguez, H. Souchon, M.-B. Lascombe, P. M. Alzari, *J. Mol. Biol.* **1996**, *257*, 1042–1051; b) C. Talotta, C. Gaeta, M. De Rosa, J. R. Ascenso, P. M. Marcos, P. Neri, *Eur. J. Org. Chem.* **2016**, 158–167.

[2] a) S. Matile, A. Vargas Jentzsch, J. Montenegro, A. Fin, *Chem. Soc. Rev.* **2011**, *40*, 2453–2474; b) S. Maiti, C. Pezzato, S. Garcia Martin, L. J. Prins, *J. Am. Chem. Soc.* **2014**, *136*, 11288–11291; c) M. J. Langton, L. M. Scriven, N. H. Williams, C. A. Hunter, *J. Am. Chem. Soc.* **2017**, *139*, 15768–15773.

[3] D. S. Sholl, R. P. Lively, *Nature* **2016**, *532*, 435–437.

[4] a) J. J. Perry IV, J. A. Perman, M. J. Zaworotko, *Chem. Soc. Rev.* **2009**, *38*, 1400 – 1417; b) T. R. Cook, Y. R. Zheng, P. J. Stang, *Chem. Rev.* **2013**, *113*, 734 – 777.

[5] a) "Functional Metal-Organic Frameworks: Gas Storage, Separation and Catalysis": M. Schroder in *Topics in Current Chemistry, Vol. 293* (Ed.: M. Schroder), Springer, Heidelberg, **2010**, pp. 1 – 262; b) L. R. MacGillivray, C. M. Lukehart, *Metal-Organic Framework Materials*, Wiley, Hoboken, **2014**.

[6] S. Kitagawa, R. Kitaura, S. Noro, *Angew. Chem. Int. Ed.* **2004**, *43*, 2334 – 2375; *Angew. Chem.* **2004**, *116*, 2388 – 2430.

[7] a) H. S. Scott, A. Bajpai, K.-J. Chen, T. Pham, B. Space, J. J. Perry, M. J. Zaworotko, *Chem. Commun.* **2015**, *51*, 14832 – 14835; b) P. Nugent, Y. Belmabkhout, S. D. Burd, A. J. Cairns, R. Luebke, K. Forrest, T. Pham, S. Ma, B. Space, L. Wojtas, M. Eddaoudi, M. J. Zaworotko, *Nature* **2013**, *495*, 80 – 84.

[8] J. D. Sherman, *Proc. Natl. Acad. Sci. USA* **1999**, *96*, 3471.

[9] B. Moulton, M. J. Zaworotko, *Chem. Rev.* **2001**, *101*, 1629 – 1658.

[10] a) A. Schneemann, V. Bon, I. Schwedler, I. Senkovska, S. Kaskel, R. A. Fischer, *Chem. Soc. Rev.* **2014**, *43*, 6062 – 6096; b) S. Horike, S. Shimomura, S. Kitagawa, *Nat. Chem.* **2009**, *1*, 695 – 704; c) G. Férey, C. Serre, *Chem. Soc. Rev.* **2009**, *38*, 1380 – 1399; d) S. K. Elsaidi, M. H. Mohamed, D. Banerjee, P. K. Thallapally, *Coord. Chem. Rev.* **2018**, *358*, 125 – 152.

[11] J. A. Mason, J. Oktawiec, M. K. Taylor, M. R. Hudson, J. Rodriguez, J. E. Bachman, M. I. Gonzalez, A. Cervellino, A. Guagliardi, C. M. Brown, P. L. Llewellyn, N. Masciocchi, J. R. Long, *Nature* **2015**, *527*, 357 – 361.

[12] H. Sato, W. Kosaka, R. Matsuda, A. Hori, Y. Hijikata, R. V. Belosludov, S. Sakaki, M. Takata, S. Kitagawa, *Science* **2014**, *343*, 167 – 170.

[13] Y. Zhang, X. Zhang, J. Lyu, K.-i. Otake, X. Wang, L. R. Redfern, C. D. Malliakas, Z. Li, T. Islamoglu, B. Wang, O. K. Farha, *J. Am. Chem. Soc.* **2018**, *140*, 11179 – 11183.

[14] R. Haldar, R. Matsuda, S. Kitagawa, S. J. George, T. K. Maji, *Angew. Chem. Int. Ed.* **2014**, *53*, 11772 – 11777; *Angew. Chem.* **2014**, *126*, 11966 – 11971.

[15] P. Horcajada, T. Chalati, C. Serre, B. Gillet, C. Sebrie, T. Baati, J. F. Eubank, D. Heurtaux, P. Clayette, C. Kreuz, J. S. Chang, Y. K. Hwang, V. Marsaud, P. N. Bories, L. Cynober, S. Gil, G. Ferey, P. Couvreur, R. Gref, *Nat. Mater.* **2010**, *9*, 172 – 178.

[16] A.-X. Zhu, Q.-Y. Yang, A. Kumar, C. Crowley, S. Mukherjee, K.-J. Chen, S.-Q. Wang, D. O'Nolan, M. Shivanna, M. J. Zaworotko, *J. Am. Chem. Soc.* **2018**, *140*, 15572 – 15576.

[17] P. Z. Moghadam, A. Li, S. B. Wiggin, A. Tao, A. G. P. Maloney, P. A. Wood, S. C. Ward, D. Fairen-Jimenez, *Chem. Mater.* **2017**, *29*, 2618 – 2625.

[18] M. Shivanna, Q.-Y. Yang, A. Bajpai, E. Patyk-Kazmierczak, M. J. Zaworotko, *Nat. Commun.* **2018**, *9*, 3080.

[19] a) M.-H. Yu, B. Space, D. Franz, W. Zhou, C. He, L. Li, R. Krishna, Z. Chang, W. Li, T.-L. Hu, X.-H. Bu, *J. Am. Chem. Soc.* **2019**, *141*, 17703 – 17712; b) A. P. Katsoulidis, D. Antypov, G. F. S. Whitehead, E. J. Carrington, D. J. Adams, N. G. Berry, G. R. Darling, M. S. Dyer, M. J. Rosseinsky, *Nature* **2019**, *565*, 213 – 217; c) H. Zeng, M. Xie, Y.-L. Huang, Y. Zhao, X.-J. Xie, J.-P. Bai, M.-Y. Wan, R. Krishna, W. Lu, D. Li, *Angew. Chem. Int. Ed.* **2019**, *58*, 8515 – 8519; *Angew. Chem.* **2019**, *131*, 8603 – 8607; d) R. Matsuda, R. Kitaura, S. Kitagawa, Y. Kubota, T. C. Kobayashi, S. Horike, M. Takata, *J. Am. Chem. Soc.* **2004**, *126*, 14063 – 14070; e) J. Tian, C. Shi, C. Xiao, F. Jiang, D. Yuan, Q. Chen, M. Hong, *Inorg. Chem.* **2020**, *59*, 18264 – 18275.

[20] a) S. Gao, C. G. Morris, Z. Lu, Y. Yan, H. G. W. Godfrey, C. Murray, C. C. Tang, K. M. Thomas, S. Yang, M. Schröder, *Chem. Mater.* **2016**, *28*, 2331 – 2340; b) J. Shen, X. He, T. Ke, R. Krishna, J. M. van Baten, R. Chen, Z. Bao, H. Xing, M. Dincă, Z. Zhang, Q. Yang, Q. Ren, *Nat. Commun.* **2020**, *11*, 6259; c) T. Ke, Q. Wang, J. Shen, J. Zhou, Z. Bao, Q. Yang, Q. Ren, *Angew. Chem. Int. Ed.* **2020**, *59*, 12725 – 12730; *Angew. Chem.* **2020**, *132*, 12825 – 12830; d) Q. Dong, X. Zhang, S. Liu, R.-B. Lin, Y. Guo, Y. Ma, A. Yonezu, R. Krishna, G. Liu, J. Duan, R. Matsuda, W. Jin, B. Chen, *Angew. Chem. Int. Ed.* **2020**, *59*, 22756 – 22762; *Angew. Chem.* **2020**, *132*, 22944 – 22950; correction: Q. Dong, X. Zhang, S. Liu, R.-B. Lin, Y. Guo, Y. Ma, A. Yonezu, R. Krishna, G. Liu, J. Duan, R. Matsuda, W. Jin, B. Chen, *Angew. Chem. Int. Ed.* **2021**, *60*, 3850 – 3850; *Angew. Chem.* **2021**, *133*, 3894 – 3894; e) R.-B. Lin, L. Li, H. Wu, H. Arman, B. Li, R.-G. Lin, W. Zhou, B. Chen, *J. Am. Chem. Soc.* **2017**, *139*, 8022 – 8028; f) R. Matsuda, R. Kitaura, S. Kitagawa, Y. Kubota, R. V. Belosludov, T. C. Kobayashi, H. Sakamoto, T. Chiba, M. Takata, Y. Kawazoe, Y. Mita, *Nature* **2005**, *436*, 238 – 241; g) J. Wang, Y. Zhang, P. Zhang, J. Hu, R.-B. Lin, Q. Deng, Z. Zeng, H. Xing, S. Deng, B. Chen, *J. Am. Chem. Soc.* **2020**, *142*, 9744 – 9751.

[21] a) G. L. Smith, J. E. Eyley, X. Han, X. Zhang, J. Li, N. M. Jacques, H. G. W. Godfrey, S. P. Argent, L. J. McCormick McPherson, S. J. Teat, Y. Cheng, M. D. Frogley, G. Cinque, S. J. Day, C. C. Tang, T. L. Easun, S. Rudić, A. J. Ramirez-Cuesta, S. Yang, M. Schröder, *Nat. Mater.* **2019**, *18*, 1358—1365; b) Y.-S. Bae, C. Y. Lee, K. C. Kim, O. K. Farha, P. Nickias, J. T. Hupp, S. T. Nguyen, R. Q. Snurr, *Angew. Chem. Int. Ed.* **2012**, *51*, 1857 – 1860; *Angew. Chem.* **2012**, *124*, 1893 – 1896.

[22] P. Li, Y. He, Y. Zhao, L. Weng, H. Wang, R. Krishna, H. Wu, W. Zhou, M. O'Keeffe, Y. Han, B. Chen, *Angew. Chem. Int. Ed.* **2015**, *54*, 574 – 577; *Angew. Chem.* **2015**, *127*, 584 – 587.

[23] Z. Zhang, S. B. Peh, Y. Wang, C. Kang, W. Fan, D. Zhao, *Angew. Chem. Int. Ed.* **2020**, *59*, 18927 – 18932; *Angew. Chem.* **2020**, *132*, 19089 – 19094.

[24] E. J. Carrington, C. A. McAnally, A. J. Fletcher, S. P. Thompson, M. Warren, L. Brammer, *Nat. Chem.* **2017**, *9*, 882 – 889.

[25] B. Li, X. L. Cui, D. O'Nolan, H. M. Wen, M. D. Jiang, R. Krishna, H. Wu, R. B. Lin, Y. S. Chen, D. Q. Yuan, H. B. Xing, W. Zhou, Q. L. Ren, G. D. Qian, M. J. Zaworotko, B. L. Chen, *Adv. Mater.* **2017**, *29*, 7.

[26] K. J. Chen, H. S. Scott, D. G. Madden, T. Pham, A. Kumar, A. Bajpai, M. Lusi, K. A. Forrest, B. Space, J. J. Perry, M. J. Zaworotko, *Chem* **2016**, *1*, 753 – 765.

[27] Z. Bao, G. Chang, H. Xing, R. Krishna, Q. Ren, B. Chen, *Energy Environ. Sci.* **2016**, *9*, 3612 – 3641.

[28] Y.-L. Peng, T. Pham, P. Li, T. Wang, Y. Chen, K.-J. Chen, K. A. Forrest, B. Space, P. Cheng, M. J. Zaworotko, Z. Zhang, *Angew. Chem. Int. Ed.* **2018**, *57*, 10971 – 10975; *Angew. Chem.* **2018**, *130*, 11137 – 11141.

[29] T. L. Hennigar, D. C. MacQuarrie, P. Losier, R. D. Rogers, M. J. Zaworotko, *Angew. Chem. Int. Ed. Engl.* **1997**, *36*, 972 – 973; *Angew. Chem.* **1997**, *109*, 1044 – 1046.

[30] A. Bajpai, D. O'Nolan, D. G. Madden, K. J. Chen, T. Pham, A. Kumar, M. Lusi, J. J. Perry, B. Space, M. J. Zaworotko, *Chem. Commun.* **2017**, *53*, 11592 – 11595.

[31] J. Gao, X. Qian, R.-B. Lin, R. Krishna, H. Wu, W. Zhou, B. Chen, *Angew. Chem. Int. Ed.* **2020**, *59*, 4396 – 4400; *Angew. Chem.* **2020**, *132*, 4426 – 4430.

[32] J. Pei, K. Shao, J.-X. Wang, H.-M. Wen, Y. Yang, Y. Cui, R. Krishna, B. Li, G. Qian, *Adv. Mater.* **2020**, *32*, 1908275.

[33] Z. Niu, X. Cui, T. Pham, G. Verma, P. C. Lan, C. Shan, H. Xing, K. A. Forrest, S. Suepaul, B. Space, A. Nafady, A. M. Al-Enizi, S. Ma, *Angew. Chem. Int. Ed.* **2021**, *60*, 5283 – 5288; *Angew. Chem.* **2021**, *133*, 5343 – 5348.

[34] H. Pan, J. A. Ritter, P. B. Balbuena, *Langmuir* **1998**, *14*, 6323 – 6327.

[35] A. L. Myers, J. M. Prausnitz, *AIChE J.* **1965**, *11*, 121 – 127.

[36] C. Gu, N. Hosono, J.-J. Zheng, Y. Sato, S. Kusaka, S. Sakaki, S. Kitagawa, *Science* **2019**, *363*, 387 – 391.

Manuscript received: May 9, 2021
Accepted manuscript online: July 12, 2021
Version of record online: August 9, 2021

